Modelling of the propagation of hydraulic fracture using cohesive zone models

Dong Liu, Brice Lecampion & Lorenzo Benedetti

Geo-Energy Lab EPFL-ENAC-IIC-GEL Staion 18 CH-1015, Switzerland

I. Introduction

Hydraulic fracturing (HF) is widely used in the oil and gas industry to enhance production from tight reservoirs. The process involves the injection of fluid at a given flow rate into a wellbore in order to propagate a fracture in rocks and thus increase their permeability.

Linear hydraulic fracture mechanics (LHFM) theories have been developped to predict the fracture propagation, assuming a linear elastic solid and the lubrication fluid flow in the fracture. However, some studies (Chudnovsky et al. 2008; Papanastasiou 1999) have shown deviations from LHFM predictions which indicates an existence of solid non-linearity and a deviation of the Poiseille law.

We revisit the problem of a plane-strain hydraulic fracture driven by the injection of a Newtonian fluid in a tight rock. By modelling the quasi-brittle nature of the rock with different cohesive zone models, we study the effect of solid non-linearity on toughness and viscosity-dominated HF regimes.

II. Problem formulation

Cohesive model	Cohesive force	Fracture energy
Dugdale-Barenblatt	$\sigma_{coh}(w) = \begin{cases} \sigma_T & w \in [0, w_c] \\ 0 & w > w_c \end{cases}$	$G_c = \sigma_T w_c$
Linear softening	$\sigma_{coh}(w) = \begin{cases} \sigma_T\,(1 - w/w_c) & w \in [0, w_c] \\ 0 & w > w_c \end{cases}$	$G_c = \sigma_T w_c/2$
Exponential Linear	$\sigma_{coh}(w) = \sigma_T \exp\left(-w/w_c\right)$	$G_c = \sigma_T w_c$
Exponential Square	$\sigma_{coh}(w) = \sigma_T \exp\left(-(w/w_c)^2\right)$	$G_c = \sqrt{\pi}\sigma_T w_c/2$

Table 1. Different cohesive zone models and their critial fracture energy

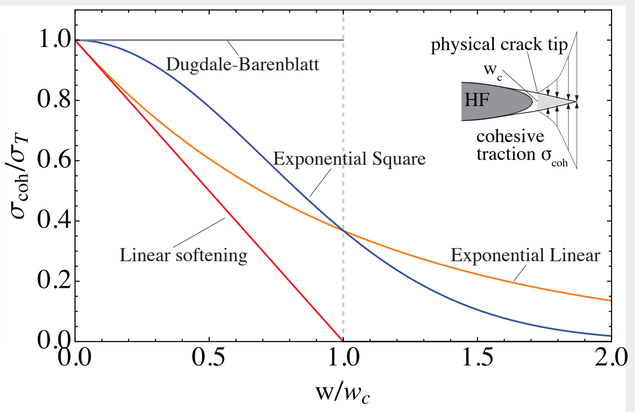

Figure 1. Traction separation laws of different cohesive zone models

Elasticity Fracture opening w is related to the net pressure (p_f-σ_o) and cohesive force σ_{coh} in the fracture [-*l*, *l*] (*l* is half fracture length including the cohesive length) via a Cauchy singular integral equation.

$$p_f(x) - \sigma_o - \sigma_{coh}(x, w) = -\frac{E'}{4\pi}\int_{-\ell}^{\ell} \frac{1}{x' - x}\frac{\partial w}{\partial x'}dx'$$

σ_{coh} is characterized by different traction-separation law, see in Figure 1 and Table 1 where σ_T represents the yielding tensile stress of the material and w_c is the critical opening in the cohesive model. $E'=E/(1-\nu^2)$ is the effective elastic modulus.

Fluid flow in the fracture If one neglects the fluid compressibility and considers a constant fluid density, by applying the Poiseuille law, the width-averaged mass conservation turns to

$$\frac{\partial w}{\partial t} - \frac{\partial}{\partial x}\left(\frac{w^3}{\mu'}\frac{\partial p}{\partial x}\right) = 0$$

where $\mu'=12\mu$, however in the case of an inviscid fluid, the mass conservation of the fluid further simplifies to

$$V_{crack} = \int_{-\ell}^{\ell} w(x)dx = Q_o t$$

Boundary condition Fluid is injected at $x=0$ at a given flow rate Q_o.

$$Q(x = 0, t) = Q_o$$

III. Numerical scheme and algorithm

A fixed regular grid is used and an implicit scheme is adopted to solve the increments of the pressure and dislocation for this fully-coupled problem. The elasticity is solved numerically using displacement discontinuity method using piece-wise linear element while the equation of mass conservation is solved by a finite volume method.

At the beginning of a time-step, at time t_n, the fracture length l_o, opening profile w_o, fluid pressure profile of p_f^o, clamping stress and cohesive forces along the crack are known. For an increment of time Δt , the solution is obtained using two nested loops. For a trial location of the fracture front, the highly non-linear fluid-solid coupling arising from the elasticity and fluid-mass conservation is solved iteratively in terms of opening and pressure increment. Once with the new opening and pressure profile, a new estimate of the fracture front is obtained by checking for the normal stress ahead of the front location. A fixed point scheme is used with under-relaxation. The sequence of increments for each given fracture front and the subsequent update of the fracture front is repeated until convergence of the fracture front estimation. During the propagation, time step can be adapted with the fracture velocity. The tip advances if normal stresses at both collocation points of one element yield the critical tensile strength σ_T in the cohesive zone model, when considering the viscosity.

IV. Results and Analysis

Scaling parameters

We compare the numerical results with the LHFM analytical solutions having the same critical fracture energy.

Toughness-dominated regime The numerical results are scaled with the parameters related to the cohesive model, keeping the critical fracture energy $G_c = \sigma_T w_c$

$$\pi = \frac{p}{\sigma_T}, \quad \gamma = \frac{l}{L^*}, \quad \tau = \frac{t}{t^*}, \quad t^* = \frac{E' w_c^2}{\sigma_T Q_o}, \quad L^* = \frac{E' w_c}{\sigma_T}$$

The evolution of the dimensionless net pressure and fracture length can be seen in Figure 2.

Viscosity-dominated regime

Similarly, we also scale respectively the opening, the net pressure, the time and the fracture length with w^*_m, p^*_m, t^*_m and L^*_m.(Detournay, E. 2004)

$$\Omega_m = \frac{w}{w_m^*}, \quad \Pi_m = \frac{p}{p_m^*}, \quad \tau_m = \frac{t}{t_m^*}, \quad \gamma_m = \frac{\ell_a}{L_m^*(t_m^*)}, \quad \xi = \frac{x}{\ell_a}$$

$$w_m^* = \frac{Q_o^{\frac{1}{2}}\mu'^{\frac{1}{6}}t^{\frac{1}{3}}}{E'^{\frac{1}{6}}}, \quad p_m^* = \frac{E'^{\frac{2}{3}}\mu'^{\frac{1}{3}}}{t^{\frac{1}{3}}}, \quad t_m^* = \frac{E'^2\mu'}{\sigma_T^3}, \quad L_m^*(t) = \frac{E'^{\frac{1}{6}}Q_o^{\frac{1}{2}}t^{\frac{2}{3}}}{\mu'^{\frac{1}{6}}}$$

where γ_m represents the dimensionless half fracture length exluding the cohesive zone length (where the opening is below the critical opening wc) and ξ represents the dimensionless coordinate. The opening and pressure profile of one time step and the evolution of the dimensionless fracture length and its relative error are shown in Figure 4.

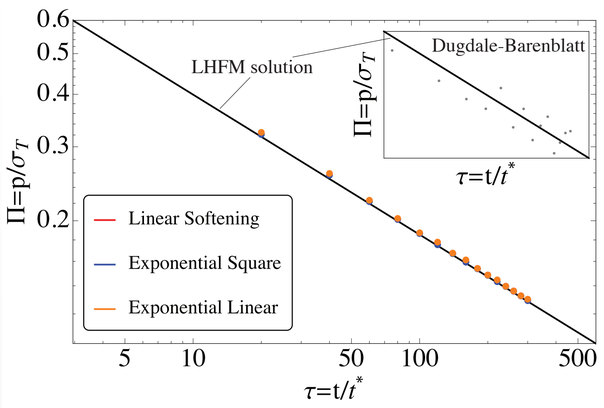

(a) Dimensionless net pressure

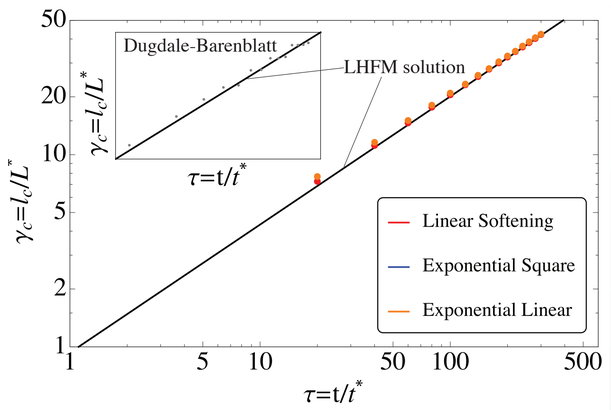

(b) Dimensionless fracture length, cohesive length included

Figure 2. Evolution of the net pressure and fracture length with time in toughness dominated regime (zero fluid viscosity) using different cohesive models with the same critical fracture energy

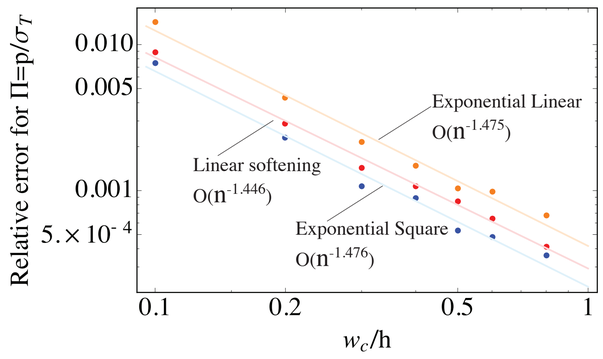

(a) Dimensionless net pressure

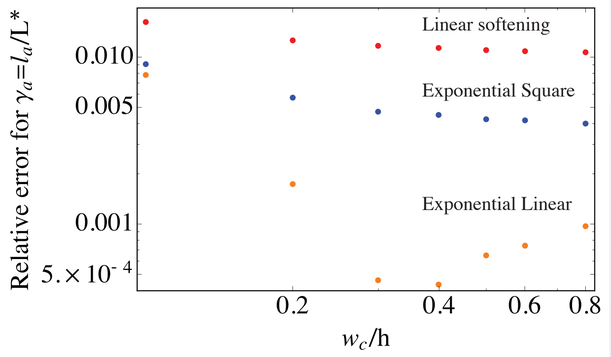

(b) Dimensionless fracture length, cohesive length excluded

Figure 3. Evolution of the relative error (average from τ=140 to τ=300) of the net pressure and fracture length with the element size *h* in toughness dominated regime (zero fluid viscosity) using different cohesive models with the same critical fracture energy

Effect of cohesive zone models

The numerical results obtained with a cohesive zone model diviates from the LHFM solution at early time, where the cohesive zone is large compared with the fracture. At large time, different cohesive models all tend to the same LHFM solutions. This indicates that the fracture energy dominates the fracture propagation regardless of the cohesive zone models. However, numerical oscillations are found during the application of Dugdale-Barenblatt model, which are not observed in the analytical solutions using Dugdale-Barenblatt model. These oscillations are not realistic and are related to the discretization of the mesh, the injection volume and the sudden drop of cohesive forces in the model.

Influence of the mesh size

The numerical accuracy relies on the mesh size, especially for the problem related to cohesive zone, where the cohesive length is small compared with the whole fracture length, but characterizes the most important critical fracture energy during the propagation. We calculate the relative error of the dimensionless net pressure and fracture length, see in Figure 3. One finds that all of these models get decreasing errors while increasing the element number, from which we can control the relative errors by playing the relation between the critical opening and the mesh size.

Figure 3 also shows the relative errors of the fracture length. Knowing that the cohesive length determines the critical fracture energy, it's more reasonable to compare the fracture length with the LHFM solutions after taking off the cohesive length (the length whose corresponding opening is below the critical opening w_c). However, this method is only correct for the linear softening model, where the cohesive length zone covers all the fracture energy. This explains the increasing relative error for the exponential linear model who has a more important part of fracture energy outside the calculated cohesive zone.

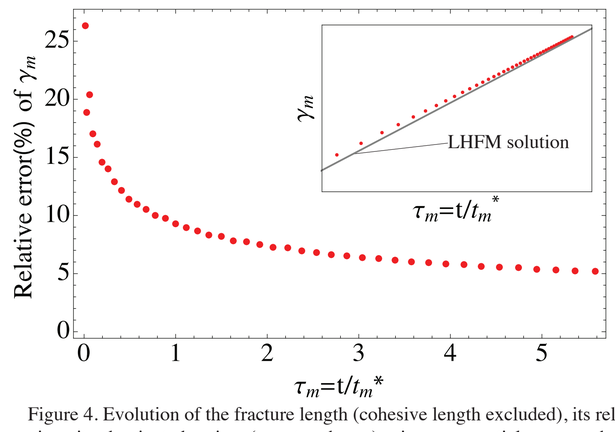

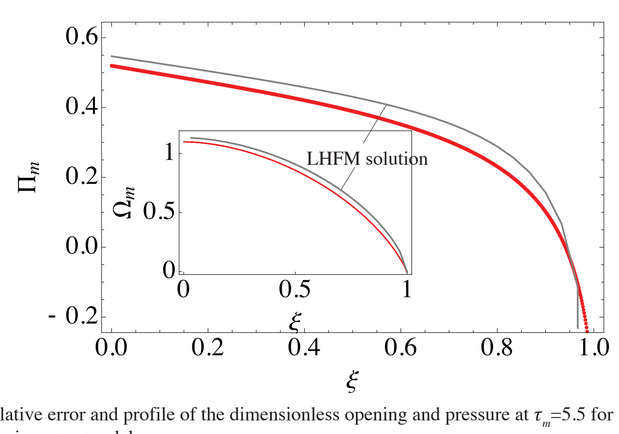

Figure 4. Evolution of the fracture length (cohesive length excluded), its relative error and profile of the dimensionless opening and pressure at τ_m=5.5 for viscosity-dominated regime (zero toughness) using exponential square cohesive zone model

V. Conclusions

1. The numerical algorithm reproduces the same results as LHFM solutions at large time when the cohesive zone is small compared to the fracture length. The shape of the material softening law or cohesive zone model does not influence the results.
2. The accuracy of this method depends on the mesh refinement in the cohesive zone, which will be costly using a fixed uniform mesh. (To reach a reasonable relative error, say 0.1%, one needs an element size of $2w_c$).

VI. Future work

Further work would be done in studying the deviation of Poiseuille law coupled with the solid non-linearity. A spectral method would be used to improve the numerical precision limited by the numerical cost of the method mentioned in this work. Moreover, a mesh-adaptive method would also be studied.

VII. References

[1] Chudnovsky, A., Fan, F., Shulkin, Y., Zhang, H., Dudley, J. & Wong, G. 2008: Hydraulic Fracture Simulation Revisited, In: 42nd US Rock Mechanics Symposium and 2nd US-Canada Rock Mechanics Symposium. ARMA.

[2] Detournay, E. 2004: Propagation regimes of fluid-driven fractures in impermeable rocks. Int J Geomech, 4(1), 35-45.

[3] Lecampion, B. 2012: Hydraulic Fracture Initiation From an Open-hole: Wellbore Size, Pressurization Rate And Fluid-solid Coupling Effects, In: 46th U.S. Rock Mechanics/Geomechanics Symposium and 6th US-Canada Rock Mechanics Symposium. ARMA.

[4] Papanastasiou, P. 1999: The effective fracture toughness in hydraulic fracturing. Int J Fracture, 96.2,127–147.

d.liu@epfl.ch